


# Exploring the mechanism of action of Huangqin Shegan Decoction in the treatment of acute pneumonia based on network pharmacology combined with transcriptomics

Ze-Bing Xia<sup>1</sup>, Yuan-Rong Zou<sup>1</sup>, Yan-Chen Wang<sup>1</sup>, Zi-Jian Zhang<sup>1</sup>, Gang Zhang<sup>1</sup>, Liang Peng<sup>1</sup>, Jing Gao<sup>1</sup>, Chang-Li Wang<sup>1</sup>, Jun-Ming Zheng<sup>2</sup>, Hong-Yan Wang<sup>3\*</sup>, Yong-Gang Yan<sup>1,4\*</sup> 

<sup>1</sup>School of Pharmacy, Shaanxi University of Chinese Medicine, Xianyang 712046, China. <sup>2</sup>Shanlin Herbal Medicine Technology Co. of Shaanxi Chengcheng County, Weinan 715200, China. <sup>3</sup>School of Acupuncture and Therapeutics, Shaanxi University of Chinese Medicine, Xianyang 712046, China. <sup>4</sup>Shaanxi Qinling Herbal Medicine Application Development Engineering and Technology Research Centre, Xianyang 712046, China.

\*Correspondence to: Hong-Yan Wang, School of Acupuncture and Therapeutics, Shaanxi University of Chinese Medicine, Xixian Avenue, Xixian New Area, Xianyang 712046, China. E-mail: Fengyun8817@163.com. Yong-Gang Yan, School of Pharmacy, Shaanxi University of Chinese Medicine, Xixian Avenue, Xixian New Area, Xianyang 712046, China. E-mail: yunfeng828@163.com.

## Author contributions

Xia ZB performed the experiment and wrote the manuscript. Zou YR, Wang YC and Zhang ZJ performed the data analyses. Zhang G and Peng L helped perform the experiment. Gao J, Wang CL and Zheng JM helped perform the analysis with constructive discussions. Wang HY and Yan YG contributed to the conception of the study.

## Competing interests

The authors declare no conflicts of interest.

## Acknowledgments

The authors would like to express their sincere gratitude to the "Qin Medicine" Quality Evaluation and Resource Development Discipline Innovation Team Project of Shaanxi University of Traditional Chinese Medicine (2019-QN01), Shaanxi University of Traditional Chinese Medicine School of Pharmacy/Shaanxi Engineering Research Centre for the Application and Development of Qinling Herbal Medicine, "Qin Medicine" Research and Development Key Laboratory (2019-QYPT-002), Shaanxi Provincial Administration of Traditional Chinese Medicine Province, Research and Development Key Laboratory (2019-QYPT-002), Shaanxi Provincial Administration of Traditional Chinese Medicine Province Chinese medicine province-wide earmarked special project: "Qin medicine planting and breeding guide research" (2021-QYZL-02), Shaanxi Provincial Science and Technology Department project: Chinese medicine *Scutellaria baicalensis* germplasm selection, seedling breeding and planting key technology research (2016KTTSSF01-01-01) and other projects. We thank Bullet Edits Limited for language editing and proofreading of the manuscript.

## Peer review information

Traditional Medicine Research thanks Hua-Chong Xu, Long Fan and another anonymous reviewer for their contribution to the peer review of this paper.

## Abbreviations

AP, acute pneumonia; HQSGD, Huangqin Shegan Decoction; TNF- $\alpha$ , tumor necrosis factor- $\alpha$ ; IL-1 $\beta$ , interleukin-1 $\beta$ ; CRP, C-reactive protein; LPS, lipopolysaccharide; ELISA, enzyme-linked immunosorbent assay; UPLC-MS/MS, ultra-performance liquid chromatography-tandem mass spectrometry; PPI, protein-protein interaction; GO, Gene Ontology; KEGG, Kyoto Encyclopedia of Genes and Genomes; DEGs, differentially expressed genes; HE, Hematoxylin-eosin; BCA, bicinchoninic acid assay; SOD, superoxide dismutase; MDA, malondialdehyde; TCM, traditional Chinese medicine; AZM, azithromycin; q-PCR, quantitative polymerase chain reaction.

## Citation

Xia ZB, Zou YR, Wang YC, et al. Exploring the mechanism of action of Huangqin Shegan Decoction in the treatment of acute pneumonia based on network pharmacology combined with transcriptomics. *Tradit Med Res*. 2025;10(7):39. doi: 10.53388/TMR20240911001.

Executive editor: Jing-Yi Wang.

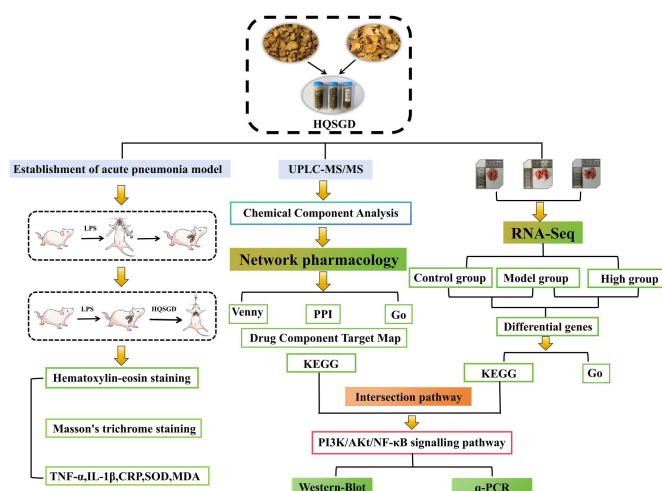
Received: 11 September 2024; Revised: 07 November 2024; Accepted: 21 November 2024; Available online: 20 December 2024.

© 2025 By Author(s). Published by TMR Publishing Group Limited. This is an open access article under the CC-BY license. (<https://creativecommons.org/licenses/by/4.0/>)

## Abstract

**Background:** In this research, we explored the operational principles of Huangqin Shegan decoction (HQSGD) for addressing acute pneumonia utilizing network pharmacology (NP) and transcriptomic analysis. **Methods:** Methods: A rat model of acute pneumonia was developed by treating rats with lipopolysaccharide (LPS) through a non-exposed tracheal drip. The pharmacological effects of HQSGD were evaluated via histopathological analysis of rat lung tissues, histological scoring of lung injury, assessment of lung index, serum inflammatory factors, oxidative stress levels, western blotting, and qRT-PCR. The active compounds of HQSGD were detected utilizing ultra-performance liquid chromatography coupled with tandem mass spectrometry (UPLC-MS/MS). NP and transcriptomic analysis were integrated to determine signaling pathways implicated in the pharmacological activity of HQSGD. The expression levels of mRNA and protein for factors implicated in these pathways were evaluated in rat lung tissues via qRT-PCR and western blotting, respectively. **Results:** HQSGD alleviated acute pneumonia in rats by reducing the lung index and the levels of TNF- $\alpha$ , IL-1 $\beta$ , CRP, and MDA while increasing the levels of SOD. The UPLC-MS/MS and NP techniques facilitated the identification of 28 bioactive constituents present in HQSGD. The principal 20 KEGG pathways were identified by intersecting the targets of HQSGD with pneumonia-related targets. These pathways were screened by comparing the transcriptomic data of the blank and model cohorts and those of the model and drug administration cohorts. GO and KEGG analyses indicated that the PI3K/AKT/NF- $\kappa$ B pathway was a potentially effective target of HQSGD. **Conclusion:** This investigation revealed the overall multi-component, multi-target, and multi-pathway interactions of HQSGD in the treatment of acute pneumonia.

**Keywords:** Huangqin Shegan Decoction; LPS; acute pneumonia; network pharmacology; transcriptomics



### Highlights

1. Huangqin Shegan Decoction exhibits significant therapeutic effects on rats with acute pneumonia.
2. The active components of Huangqin Shegan Decoction were identified using UPLC-MS/MS technology. Through the integration of network pharmacology and transcriptome sequencing technology, it was concluded that the PI3K/Akt/NF- $\kappa$ B pathway may be a molecular target for exerting therapeutic effects. Additionally, experimental studies have confirmed that the PI3K/Akt/NF- $\kappa$ B signaling pathway plays a significant negative regulatory role in pulmonary inflammatory responses.
3. The study of drugs targeting the PI3K/AKT/NF- $\kappa$ B signaling pathway for the treatment of acute pneumonia holds great promise and can pave the way for more innovative approaches in the treatment of acute pneumonia.

### Medical history of objective

Huangqin Shegan Decoction originates from the medical book "Yi Chao Lei Bian" written by the Qing Dynasty physician Weng Zao, specifically in Volume 12 (Throat and Pharynx Section). The formula consists of two Chinese medicinal herbs, *Scutellariae Radix* (Huangqin) and *Belamcandae Rhizoma* (Shegan), which are decocted in water for oral administration. It is used to treat throat odor caused by heat toxins in the lung and stomach meridians (the accumulation of heat toxins in the lung and stomach meridians leads to symptoms of a fishy odor in the throat).

### Background

Acute pneumonia (AP) is a common respiratory infection caused by bacteria, respiratory viruses, or fungi. The pathogenesis of AP is complex and characterized by a rapid onset of symptoms. In severe cases, AP can lead to cardiovascular failure, posing a life-threatening risk to patients [1]. AP is categorized as an epidemic in traditional Chinese medicine (TCM). According to Yu Jiaqian's "Epidemiology", pneumonia is classified as a wind-warmth lung-heat disease characterized by lung stasis caused by pathogenic wind-heat (Wind-warmth lung-heat: Acute febrile diseases caused by the invasion of exogenous wind-heat pathogens leading to heat in the lungs, manifested by symptoms such as fever, cough, and thick, yellow phlegm. Pathogenic wind-heat: The combination of wind and heat evils invading the human body leads to a range of symptoms.) [2]. AP is closely associated with an uncontrolled inflammatory response following infection, which leads to a poor prognosis. Pathologically, AP manifests as pulmonary inflammation, oxidative damage, and apoptosis. It has high morbidity and mortality rates and accounts for more than 50% of all pneumonia cases. Moreover, it can progress to severe pneumonia, resulting in life-threatening consequences [3, 4].

Huangqin Shegan decoction (HQSGD), documented in the medical compendium "Yi Chao Lei Bian" by physician Weng Zao from the Qing Dynasty, is a traditional Chinese herbal formulation comprising *Scutellariae Radix* (Huangqin) and *Belamcandae Rhizoma* (Shegan) that is widely used to reduce foul throat odor caused by heat-toxins affecting the lung and stomach meridians [5]. Huangqin, the dried root of *Scutellaria baicalensis* Georgi belonging to the family Labiatae, is rich in flavonoids, terpenoids, volatile oils, polysaccharides, and other compounds. Flavonoids, the main active components of Huangqin, are reported to have anti-inflammatory, antibacterial, and antiviral properties [6–8]. Shegan, the rhizome of *Belamcanda chinensis* (L.) DC, primarily contains iris glycosides, irisin, and other flavonoids that have anti-inflammatory, antioxidant, and antibacterial properties [9–11].

Cyberpharmacology is an interdisciplinary field that helps investigate drug-target relationships through complex networks of gene or protein interactions [12]. Transcriptomic techniques are used

to examine the transcriptome, a complete set of all RNA transcripts in an organism, and identify differentially expressed genes (DEGs) between healthy and diseased states [13]. Integrating network pharmacology (NP) with transcriptomic analysis represents an effective approach to identifying the active compounds and mechanisms of action of traditional herbal formulations [14–16].

Modern pharmacodynamic investigations have demonstrated that HQSGD exhibits anti-inflammatory, antibacterial, and antiviral effects on the respiratory tract [17–19]. Although the pharmacological effects of individual herbal constituents of HQSGD have been investigated at the molecular level, their specific mechanisms of action in treating AP and the intricate interaction network of these mechanisms remain unclear. Therefore, in this study, we integrated NP with transcriptomic analysis to examine the operational mechanism of HQSGD in addressing AP. Animal experiments validated the results to provide a foundation for further research.

### Materials and methods

#### Reagents

Lipopolysaccharide (LPS) was procured from Sigma Co., Ltd (St. Louis, MI, USA), (*Escherichia coli*, O55:B5, L2880-100MG). Rat TNF- $\alpha$  (MM-0180R1), IL-1 $\beta$  (MM-0047R1), and CRP (MM-0061R1) enzyme-linked immunosorbent assay (ELISA) kits were procured from Shanghai Enzyme-linked Biotechnology Co., Ltd. (Shanghai, China). Rat superoxide dismutase (SOD) (A001-3-2) and malondialdehyde (MDA) (A003-1-2) assay kits were acquired from Nanjing Jiancheng Bioengineering Institute (Nanjing, China). A bicinchoninic acid assay (BCA) assay kit (A003-2-1) was procured from Beijing Solarbio Science & Technology Co., Ltd. (Beijing, China). PI3K (60225-1-Ig), AKT (10176-2-AP), NF- $\kappa$ B (10745-1-AP), and p-NF- $\kappa$ B (82335-1-RR) were procured from Proteintech (Rosemont, IL, USA). p-PI3K (AP0854) was procured from ABclonal (Woburn, MA, USA). p-AKT (ET1607-73) was procured from HUABIO (Hangzhou, China). PCR primers were procured from Sangon Biotech (Shanghai) Co., Ltd. (Shanghai, China).

#### Animals and models

A sum of 66 healthy male SD rats of specific-pathogen-free grade (age, 7–8 weeks; weight, 200  $\pm$  30 g) were utilized in this investigation. Rats were purchased from Chengdu Dashuo Experimental Animal Co., Ltd. (Chengdu, China), with the license number: SCXK (Chuan) 2020-0030. The animals were housed in the Animal Breeding Room of Clinical Traditional Chinese Medicine at Shaanxi University of Chinese Medicine, with a room temperature of (23  $\pm$  2) °C, relative humidity of 50%–60%, and a 12 h light-dark cycle. All experimental animals were approved by the Animal Ethics Committee of Shaanxi University of Chinese Medicine. The animal ethics approval number is: SUCMDL-20231201002. All experimental procedures involving animals adhered strictly to established protocols for laboratory animal care and handling. Following a 7-day adaptation period, the rats were arbitrarily allocated into the following cohorts, with 11 rats in each cohort: control, model, low-dose (1.8 g/kg) HQSGD, medium-dose (7.2 g/kg) HQSGD, high-dose (14.4 g/kg) HQSGD, and positive-control (8 mg/kg azithromycin (AZM)) [20]. Rats in all cohorts except the control cohort underwent intratracheal instillation. Briefly, the rats were anesthetized and placed on a plate inclined at 45°, with their heads facing upward and perpendicular to the operating table. The tongue was gently pulled with forceps to expose the oral cavity, which was visualized using a smart device adjusted at an optimal angle. A pipette gun loaded with LPS (5 mg/kg) was inserted, and the solution was carefully delivered near the opening of the trachea [21]. The nose was immediately pinched to ensure inhalation. After 10 seconds, the tongue and nose were gently released, and a slight tracheal rumble indicated successful administration [22].

After successful modeling, rats in the low, medium, and high-dose HQSGD cohorts were administered 1.8 g/kg, 7.2 g/kg, and 14.4 g/kg HQSGD, correspondingly, via gavage once per day over 4 days [23].

Rats in the control and model cohorts received an equivalent volume of 0.9% saline, whereas those in the positive-control cohort were treated with 8 mg/kg AZM. After 1 h of the last dose, rats were anesthetized via intraperitoneal injection of sodium pentobarbital. Subsequently, blood was obtained from the abdominal aorta, and the lungs were extracted. The rats were ultimately placed in a carbon dioxide euthanasia chamber, where they were humanely euthanized using a method of carbon dioxide anesthesia.

The detailed protocol of animal modeling and treatment is depicted in Figure 1 (Flow chart of animal modeling and treatment). According to the 2020 edition of the Chinese Pharmacopoeia, the maximum clinical dose of HQSGD for humans is 10 g. The respective animal-equivalent doses for the three HQSGD cohorts were calculated utilizing the body weight (BW) of rats in each cohort.

#### Preparation and analysis of HQSGD

The chemical composition of HQSGD was examined utilizing ultra-performance liquid chromatography (ExionLCTM AD, <https://sciex.com.cn/>) in conjunction with ultra-performance liquid chromatography-tandem mass spectrometry (UPLC-MS/MS). The herbal constituents of HQSGD were purchased from Huiyuan Pharmacy (Xianyang, China). The herbs were authenticated by Professor Ji-Tao Wang from Shaanxi University of Traditional Chinese Medicine. Huangqin and Shegan were decocted twice with water in a 1:1 ratio [24]. The specific components of HQSGD are listed in Table 1 (List of herbal constituents of HQSGD). For the first decoction, the herbs were mixed with 8 times the amount of water and boiled for 1 h. After the solution was filtered, the herbs were decocted with 6 times the amount of water for 40 min. Filtrates from both decoctions were combined and concentrated until the concentration of the crude drug in the solution reached 1 g/mL. All extracts were maintained at  $-20^{\circ}\text{C}$  pending subsequent analysis [24]. For UPLC-MS/MS examination, HQSGD extracts were thawed and vortexed for 10 seconds. Thereafter, 100  $\mu\text{L}$  of the extract was pipetted into a 1.5 mL centrifuge tube and

combined with 100  $\mu\text{L}$  of 70% methanol containing an internal standard extract. If the volume of HQSGD was  $< 100 \mu\text{L}$ , the extract was added in a 1:1 (v/v) ratio. The mixture was vortexed at 12,000 rpm for 15 min at  $4^{\circ}\text{C}$  and centrifuged for 3 min. The liquid above the sediment was passed through a  $0.22 \mu\text{m}$  filter and kept in an injection vial for UPLC-MS/MS examination [25].

An Agilent SB-C18 column (Agilent Technologies Inc., Santa Clara, CA, USA;  $1.8 \mu\text{m}$ ,  $2.1 \text{ mm} \times 100 \text{ mm}$ ) was utilized for UPLC. Mobile phase A comprised 0.1% formic acid in ultrapure water, whereas mobile phase B comprised 0.1% formic acid in acetonitrile. Elution was initiated with 5% B at 0.00 min, progressively rising to 95% B across 9.00 min, and was maintained at 95% B for 1 min. Afterward, the proportion of B was reduced to 5% from 10.00 to 11.10 min and maintained at 5% for 14 min to achieve equilibration. Other parameters were established as below: flow rate, 0.35 mL/min; column temperature,  $40^{\circ}\text{C}$ ; injection volume, 2  $\mu\text{L}$  [26].

#### Lung morphology and pathology

The left lung lobes were halved, fixed in picric acid solution for 24 h, dehydrated, cleared, encased in paraffin, sliced to  $5 \mu\text{m}$  thickness, and stained with haematoxylin-eosin (HE). These sections were then analyzed under light microscopy to evaluate the pathological and morphological alterations in the rat lung tissues. The stained tissues were observed and photographed at  $200\times$  magnification. The tissues were graded according to the International Harmonization of Nomenclature and Diagnostic Criteria (INHAND) to evaluate pathological changes. The results of the grading are presented in Table 2 (Histopathological scoring of rat lung tissues).

#### Body mass and lung index

The alterations in rat body mass before and after modeling were calculated as follows = body mass after modeling – body mass before modeling. The rats' lung index (%) was computed as: lung mass/body mass  $\times 100\%$ .

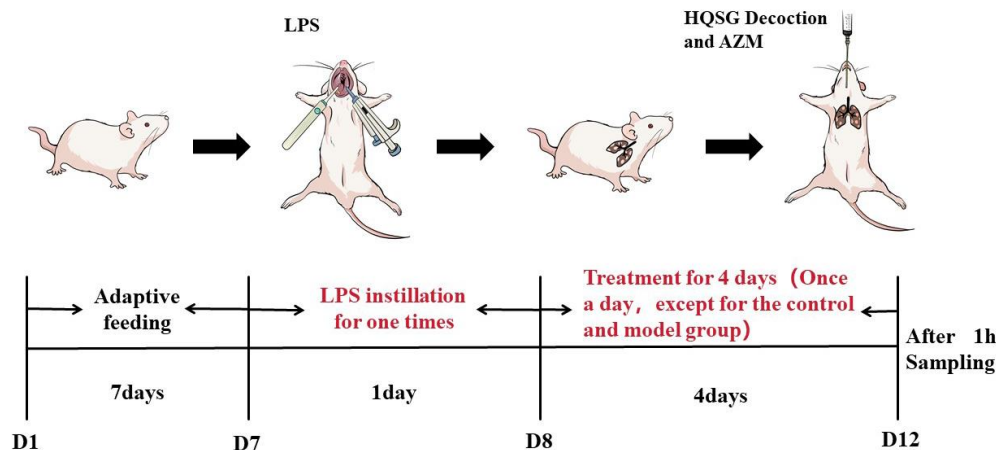


Figure 1 Flow chart of animal modelling and treatment. LPS, lipopolysaccharide.

Table 1 The list of herbal compositions in HQSGD

Herbal name in Chinese	Herbal name in the Plant List	Dosage
Huangqin	<i>Scutellaria baicalensis</i> Georgi	250 g
Shegan	<i>Belamcanda chinensis</i> (L.) DC.	250 g

Table 2 Histopathological scoring of rat lung tissues

Grade (number)	Species	Description
0	Within normal range	Tissues were considered normal when accounting for factors such as the age, sex, and strain of the animals. Deviations observed under other conditions were considered abnormal.
1	Very slight	Observed changes exceeded the normal range.
2	Slight	Lesions were observed but were not severe.
3	Moderate	Lesions were pronounced and were likely to worsen.
4	Severe	Lesions were extremely severe (affected the entire tissue or organ).

### ELISA in AP rats

The tumor necrosis factor- $\alpha$  (TNF- $\alpha$ ), interleukin-1 $\beta$  (IL-1 $\beta$ ), and C-reactive protein (CRP) levels in rat serum were detected utilizing the corresponding ELISA kits per the supplier's protocol. To assess oxidative stress levels, rat lung tissues were homogenized, and total protein was detected utilizing a BCA assay kit. Afterward, the levels of SOD and MDA in lung tissue homogenates were evaluated using corresponding assay kits per the supplier's protocol.

### Analysis of pharmacological networks

Identification of 28 active ingredients in HQSGD using the UPLC-MS/MS coupled technique. Access the PubChem database (<https://pubchem.ncbi.nlm.nih.gov/>) and import data from the SwissTargetPrediction database (<http://www.swisstargetprediction.ch/>) [27]. Duplicates were eliminated to obtain a list of potential targets of HQSGD. In addition, the keyword "acute pneumonia" was used to identify AP-specific targets in the GeneCards database ([www.genecards.org/](http://www.genecards.org/)) and OMIM database (<https://www.omim.org/>) [28]. Finally, the Venny (version 2.1.0) tool (<https://bioinfogp.cnb.csic.es/tools/venny/index.html>) was utilized to create a Venn diagram to intersect the potential targets of HQSGD with AP-specific targets.

### Construction of the protein-protein interaction (PPI) network

The intersecting targets identified in the Venn diagram were entered into the STRING database (<https://www.string-db.org/>) to generate a PPI network, with the organism being designated as "*Homo sapiens*" and the interaction score being established at 0.9 and adjusted the confidence to hide the free proteins in the network [29]. Subsequently, the network was rendered visually employing Cytoscape (version 3.8.0) software. The PPI network was developed utilizing the key targets, incorporating topological parameter degree > averaged degree values of each node.

### Analysis of Gene Ontology (GO) and Kyoto Encyclopedia of Genes and Genomes (KEGG) enrichment

GO and KEGG enrichment analyses were performed to predict potential biological functions and regulatory molecular pathways of HQSGD using David (<https://david.ncifcrf.gov/>) enrichment analyses of overlapping targets [30]. The cut-off species for the KEGG pathway enrichment analysis was *Homo sapiens* and the threshold was set at  $P < 0.01$  [31]. In GO analysis, the overlapping target genes were categorized into three domains, namely, biological processes, molecular functions, and cellular components.

### Sequencing of the transcriptome

Lung tissue specimens were procured from rats in the control, model, and high-dose HQSGD cohorts. The samples were sent to Guangzhou Kidio Biotechnology Co., Ltd. (Guangzhou, China) for RNA extraction and sequencing and were analyzed using an online analysis platform developed by the company. The company measured the RNA's quality and quantity utilizing a NanoPhotometer spectrophotometer, a Qubit 2.0 fluorometer, and an Agilent 2100 Bioanalyzer. Furthermore, we identified DEGs between the control and model cohorts and between

the high-dose HQSGD and model cohorts using FDR values of  $< 0.05$  and  $|\log_2 \text{fold change}|$  values of  $> 1$  as the screening criteria. Volcano plots and heat maps were generated to visualize both sets of DEGs. Subsequently, the DEGs underwent functional annotation through GO and KEGG pathway enrichment analyses. The KEGG pathways linked to both sets of DEGs were intersected with those associated with the overlapping target genes. Based on the ranking of the three KEGG enriched pathways and the upstream and downstream relationships of the pathways, the most relevant pathways were identified and further validated for follow-up.

### Western blotting

To extract total protein, 20 mg of rat lung tissue was ground and lysed in RIPA buffer (Beijing Solarbio Science & Technology Co., Ltd., Beijing, China). Protein concentration was detected utilizing a BCA assay kit. The protein specimens were adjusted to the same concentration as the protein sample solution and heated at a high temperature until denaturation occurred. The isolated proteins were shifted onto a PVDF membrane utilizing the wet transfer technique. The membrane was treated with 5% skimmed milk to inhibit non-specific binding, succeeded by overnight incubation at 4 °C with primary antibodies targeting PI3K (Proteintech, Rosemont, IL, USA), p-PI3K (ABclonal, Woburn, MA, USA), AKT (Proteintech, Rosemont, IL, USA), p-AKT (HUABIO, Hangzhou, China), NF- $\kappa$ B (Proteintech, Rosemont, IL, USA), p-NF- $\kappa$ B (Proteintech, Rosemont, IL, USA), and GAPDH (Abcam, Cambridge, United Kingdom). The following day, the membrane underwent rinsing with TBST buffer (Beijing Solarbio Science & Technology Co., Ltd., Beijing, China) and was then exposed to a horseradish peroxidase (HRP)-linked secondary antibody (Proteintech, Rosemont, IL, USA; 1:10,000) for 60 min at ambient condition. Thereafter, the membrane was rinsed with TBST buffer and stained. Protein bands were identified utilizing an enhanced chemiluminescence system, and the comparative protein levels of genes of interest were evaluated employing ImageJ 1.8.0.345 software, with *GAPDH* functioning as the internal reference gene. The assay was conducted in triplicate.

### Quantitative polymerase chain reaction (q-PCR)

RNA was isolated from rat lung specimens utilizing the Trizol reagent (TRANS, Cairo, Egypt). The RNA was then transformed into cDNA through reverse transcription and q-PCR analysis employing the SYBR Green Real-time PCR Master Mix kit. The comparative mRNA levels of *PI3K*, *AKT*, and *NF- $\kappa$ B* were determined utilizing the  $2^{-\Delta\Delta Ct}$  methodology, with *GAPDH* functioning as the internal control gene. The primer sequences employed for target gene amplification are depicted in Table 3.

### Statistical analysis

The statistical examination was conducted utilizing GradPad Prism (version 9.0) and SPSS Statistics (version 25.0) programs. All findings were presented as the ( $\bar{x} \pm s$ ). Comparisons between two groups employed a t-test, while evaluations across three or more cohorts applied one-way ANOVA. A  $P$ -value of  $< 0.05$  deemed statistically significant differences.

Table 3 Primer sequences for target genes

Gene name	Primer name	Primer sequence (5'-3')	Product length/bp
<i>GADPH</i>	rat-GAPDH-F	GCTTCTACGGTGCGGAGATTGTGT	188
	rat-GAPDH-R	GCCTGCTTCACCACCTTCTTGA	
<i>PI3K</i>	rat-PI3K-F	TCCTACAGTCCTATCCAATGA	197
	rat-PI3K-R	CGTCCTTCACAATCTCTATCA	
<i>AKT</i>	rat-AKT-F	TACAACCAGGACCATGAGAA	206
	rat-AKT-R	TCATACACATCTTGCCACAC	
<i>NF-<math>\kappa</math>B</i>	rat-NF- $\kappa$ B-F	GGAAGACAAGGAAGAGGATG	199
	rat-NF- $\kappa$ B-R	GTGGATGATGGCTAAGTGTA	



## Results

### Chemical ingredients analysis of HQSGD

The chemical ingredients of HQSGD were examined via UPLC-MS/MS. Mass spectral data was evaluated utilizing the Analyst (version 1.6.3) software. The total ion current (TIC) chromatogram shown in Figure 2 represents the aggregate of ion intensities in the mass spectra as a function of time. Eventually, a total of 2,715 active ingredients of HQSGD were identified via UPLC-MS/MS in Supplementary Table S1. These ingredients were screened based on oral bioavailability values of  $\geq 30\%$  and drug-like properties values of  $\geq 0.18$  in the TCMSP database. The ingredients selected based on the aforementioned criteria were integrated with those identified from a literature search in the CNKI and PubMed databases, resulting in the identification of 28 potent active ingredients (Table 4).

### Histopathological changes in rat lungs

A rat model of AP was established via intratracheal instillation of LPS without exposure. HE and Masson staining techniques assessed histopathological alterations in rat lung specimens. HE staining of lung tissues from the model cohort revealed congested airway walls and alveoli, thickened alveolar septa, an increased abundance of interstitial neutrophils, marked infiltration of inflammatory cells, and damage to alveolar epithelial cells. In contrast to the model cohort, the HQSGD and AZM cohorts had a lower proportion of interstitial granulocytes and inflammatory cells and showed significant improvements in the morphological features of alveolar epithelial

cells and alveoli (Figure 3A). Furthermore, histopathological scores were notably elevated in the model cohort relative to the control cohort and substantially diminished in the HQSGD cohort relative to the model cohort (Figure 3C).

Masson staining indicated that the deposition of collagen fibers (stained blue) in rat lung tissue's alveolar septum and interstitium was more pronounced in the model cohort relative to the control cohort. However, both collagen fiber deposition and lung fibrosis were less severe in the HQSGD cohort than in the model cohort (Figure 3B). Additionally, rats in the model cohort exhibited compromised health and experienced notable alterations in BW. Specifically, the BW of rats was markedly elevated ( $P < 0.05$ ) in the high-dose HQSGD cohort compared to the model cohort (Figure 3D). The lung index, which was computed by comparing lung tissue mass with BW, was substantially elevated in the model cohort relative to the control cohort ( $P < 0.001$ ) but considerably diminished in the high-dose HQSGD cohort relative to the model cohort ( $P < 0.05$ ). In particular, the lung index showed a decreasing trend in all HQSGD-treated and AZM cohorts (Figure 3E). These results suggested that HQSGD alleviated lung damage in rats with AP.

### Analysis of serum inflammatory factors and oxidative stress indicators

TNF- $\alpha$ , IL-1 $\beta$ , and CRP serum levels were markedly elevated in the model cohort relative to the control cohort but substantially diminished in the AZM and high-dose HQSGD cohorts relative to the model cohort (Figure 4A–4C). SOD activity in lung tissues was notably

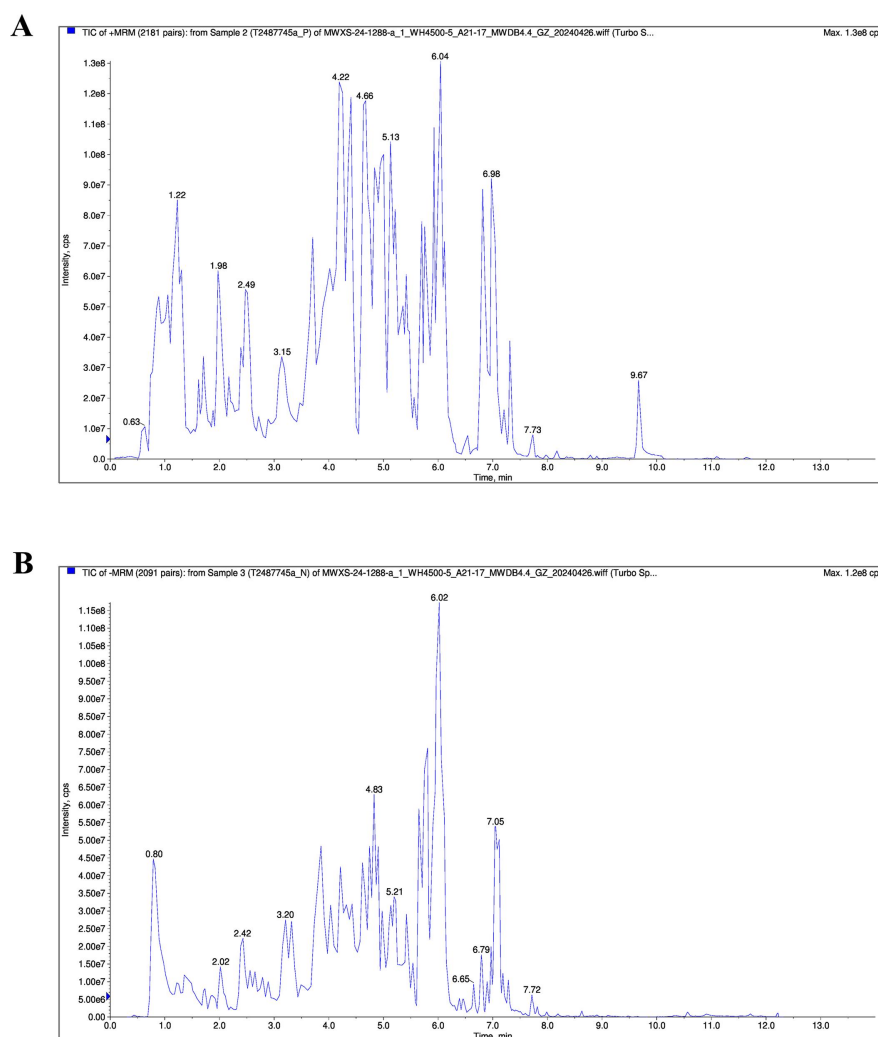


**Figure 2** UPLC-MS/MS analysis of HQSGD. (A) Chromatogram in the positive ion mode. (B) Chromatogram in the negative ion mode. The x-axis indicates the retention time of metabolites, whereas the y-axis indicates the intensity of the ion current in counts per second (Cps).

Submit a manuscript: <https://www.tmrjournals.com/tmr>

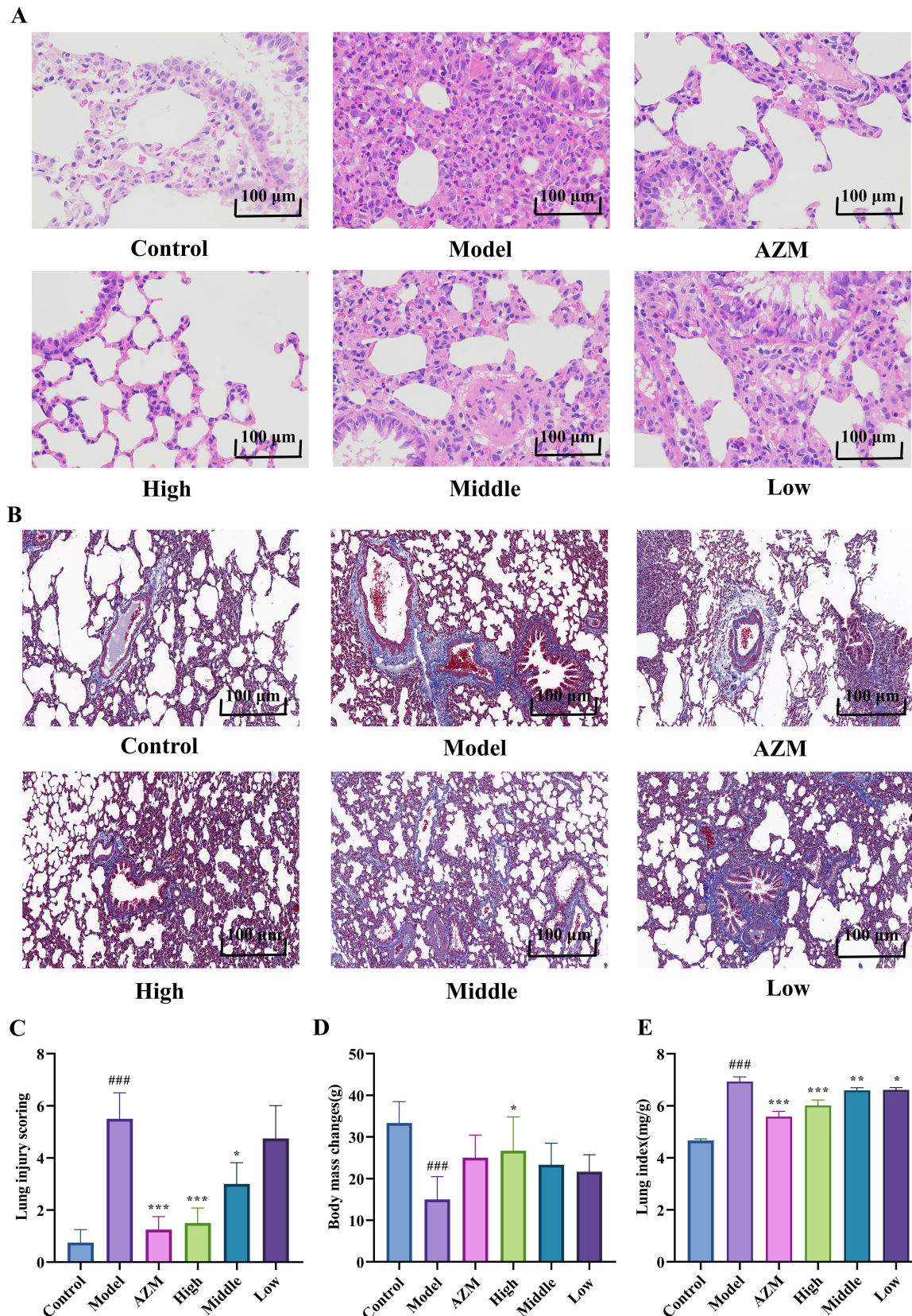


**Figure 3** HQSGD counteracted pathological changes in the lungs of rats with acute pneumonia. (A) HE staining ( $\times 200$ , scale bar = 100  $\mu\text{m}$ ). (B) Masson staining ( $\times 200$ , scale bar = 100  $\mu\text{m}$ ). (C) Histopathological scores of rat lung tissues. (D) Changes in body mass. (E) Changes in the lung index. <sup>###</sup> $P < 0.001$  vs control group; <sup>\*</sup> $P < 0.05$ , <sup>\*\*</sup> $P < 0.01$ , <sup>\*\*\*</sup> $P < 0.001$  vs model group;  $n = 6$ . AZM, azithromycin.

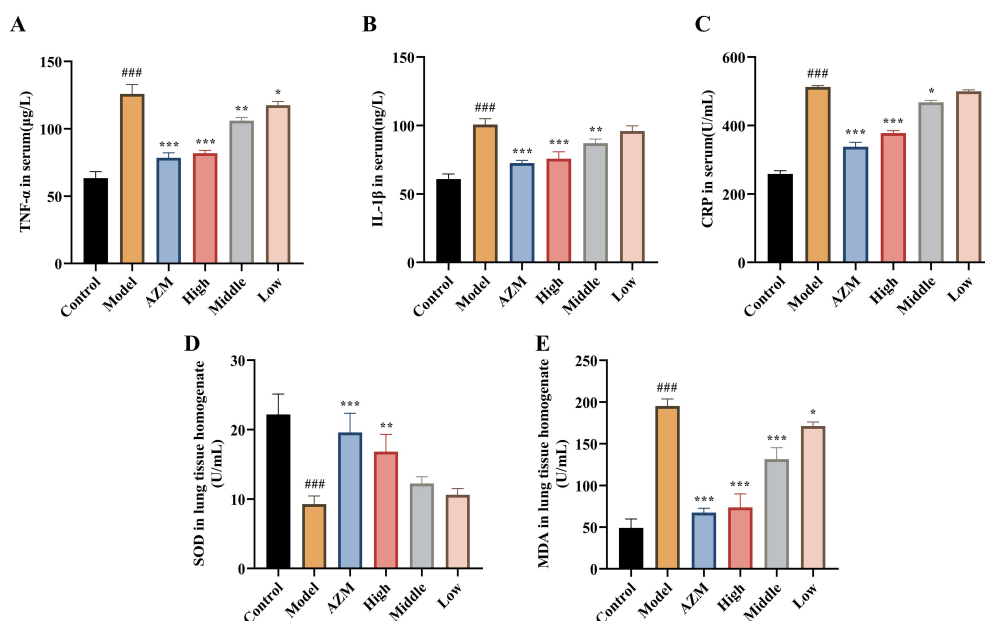


**Figure 4** HQSGD restored the levels of inflammatory factors in the serum and those of oxidative stress indicators in lung tissues in rats with acute pneumonia. (A) Serum levels of TNF- $\alpha$ . (B) Serum levels of IL-1 $\beta$ . (C) Serum levels of CRP. (D) Activity of SOD in lung tissue homogenates. (E) Expression of MDA in lung tissue homogenates. ### $P < 0.001$  vs control group; \* $P < 0.05$ , \*\* $P < 0.01$ , \*\*\* $P < 0.001$  vs model group;  $n = 6$ . AZM, azithromycin; TNF- $\alpha$ , tumor necrosis factor- $\alpha$ ; IL-1 $\beta$ , interleukin-1 $\beta$ ; CRP, C-reactive protein; SOD, superoxide dismutase; MDA, malondialdehyde.

**Table 4 28 ingredients of HQSGD**

Number	Compounds	Formula	CAS	Molecular weight (Da)
1	Baicalin	C <sub>21</sub> H <sub>18</sub> O <sub>11</sub>	21967-41-9	446.08
2	Baicalein	C <sub>15</sub> H <sub>10</sub> O <sub>5</sub>	491-67-8	270.05
3	Wogonin-7-O-Glucuronide (Wogonoside)	C <sub>22</sub> H <sub>20</sub> O <sub>11</sub>	51059-44-0	460.10
4	Wogonin (5,7-Dihydroxy-8-Methoxyflavone)	C <sub>16</sub> H <sub>12</sub> O <sub>5</sub>	632-85-9	284.07
5	Scutellarein-7-O-glucuronide (Scutellarin)*	C <sub>21</sub> H <sub>18</sub> O <sub>12</sub>	27740-01-8	462.08
6	Scutellarein (5,6,7,4'-Tetrahydroxyflavone)	C <sub>15</sub> H <sub>10</sub> O <sub>6</sub>	529-53-3	286.05
7	Tectorigenin*	C <sub>16</sub> H <sub>12</sub> O <sub>6</sub>	548-77-6	300.06
8	Tectoridin*	C <sub>22</sub> H <sub>22</sub> O <sub>11</sub>	611-40-5	462.12
9	Skullcapflavone II	C <sub>19</sub> H <sub>18</sub> O <sub>8</sub>	55084-08-7	374.10
10	Acacetin*	C <sub>16</sub> H <sub>12</sub> O <sub>5</sub>	480-44-4	284.07
11	Luteolin (5,7,3',4'-Tetrahydroxyflavone)*	C <sub>15</sub> H <sub>10</sub> O <sub>6</sub>	491-70-3	286.05
12	Taxifolin (Dihydroquercetin)	C <sub>15</sub> H <sub>12</sub> O <sub>7</sub>	480-18-2	304.06
13	Rivularin*	C <sub>18</sub> H <sub>16</sub> O <sub>7</sub>	70028-59-0	344.09
14	Resveratrol	C <sub>14</sub> H <sub>12</sub> O <sub>3</sub>	501-36-0	228.08
15	Irisflorentin	C <sub>20</sub> H <sub>18</sub> O <sub>8</sub>	41743-73-1	386.10
16	Mangiferin	C <sub>19</sub> H <sub>18</sub> O <sub>11</sub>	4773-96-0	422.08
17	Kaempferol (3,5,7,4'-Tetrahydroxyflavone)	C <sub>15</sub> H <sub>10</sub> O <sub>6</sub>	520-18-3	286.05
18	Isorhapontigenin*	C <sub>15</sub> H <sub>14</sub> O <sub>4</sub>	32507-66-7	258.09
19	Isorhamnetin; 3'-Methoxy-3,4',5,7-Tetrahydroxyflavone	C <sub>16</sub> H <sub>12</sub> O <sub>7</sub>	480-19-3	316.06
20	Iristectorin B	C <sub>23</sub> H <sub>24</sub> O <sub>12</sub>	94396-09-5	492.13
21	Eriodictyol (5,7,3',4'-Tetrahydroxyflavanone)	C <sub>15</sub> H <sub>12</sub> O <sub>6</sub>	552-58-9	288.06
22	Dimethylmatairesinol	C <sub>22</sub> H <sub>26</sub> O <sub>6</sub>	25488-59-9	386.17
23	Dihydrobaicalein	C <sub>15</sub> H <sub>12</sub> O <sub>5</sub>	35683-17-1	272.07
24	Chrysin-8-C-glucoside	C <sub>21</sub> H <sub>20</sub> O <sub>9</sub>	160880-89-7	416.11
25	Chrysin-7-O-Glucuronide	C <sub>21</sub> H <sub>18</sub> O <sub>10</sub>	35775-49-6	430.09
26	Chrysin-6-C-arabinoside-8-C-glucoside	C <sub>26</sub> H <sub>28</sub> O <sub>13</sub>	185145-33-9	548.15
27	Chrysin	C <sub>15</sub> H <sub>10</sub> O <sub>4</sub>	480-40-0	254.06
28	Norwogonin	C <sub>15</sub> H <sub>10</sub> O <sub>5</sub>	4443-09-8	270.05

\*: The presence of an asterisk in the name of a metabolite indicates that the detection results include isomers that cannot be distinguished from the substance, which are marked with an asterisk.



reduced in the model cohort relative to the control cohort but remarkably higher in the AZM and high-dose HQSGD cohorts than in the model cohort (Figure 4D). MDA expression in lung tissues was markedly elevated in the model cohort versus the control cohort but significantly lower in the AZM and high-dose HQSGD cohorts than in the model cohort (Figure 4E).

### Prediction of targets of HQSGD via NP

A total of 28 active compounds of HQSGD were identified via UPLC-MS/MS and NP. By de-weighting and combining the two approaches, 645 potential targets of HQSGD were identified.

Additionally, 780 AP-related targets were identified. A Venn diagram was generated to intersect the two sets of targets, resulting in the identification of 220 overlapping (common) targets (Figure 5A). A PPI network of these overlapping targets was generated utilizing the STRING database and depicted through the Cytoscape (version 3.8.0) software (Figure 5B), followed by mapping of an active compound-target network (Figure 5C). Subsequently, the possible mode of action of HQSGD in addressing AP was investigated using the DAVID 2021 online platform. The top 10 GO terms and the top 20 KEGG pathways linked to the target genes are depicted in Figure 5D, 5E, respectively.

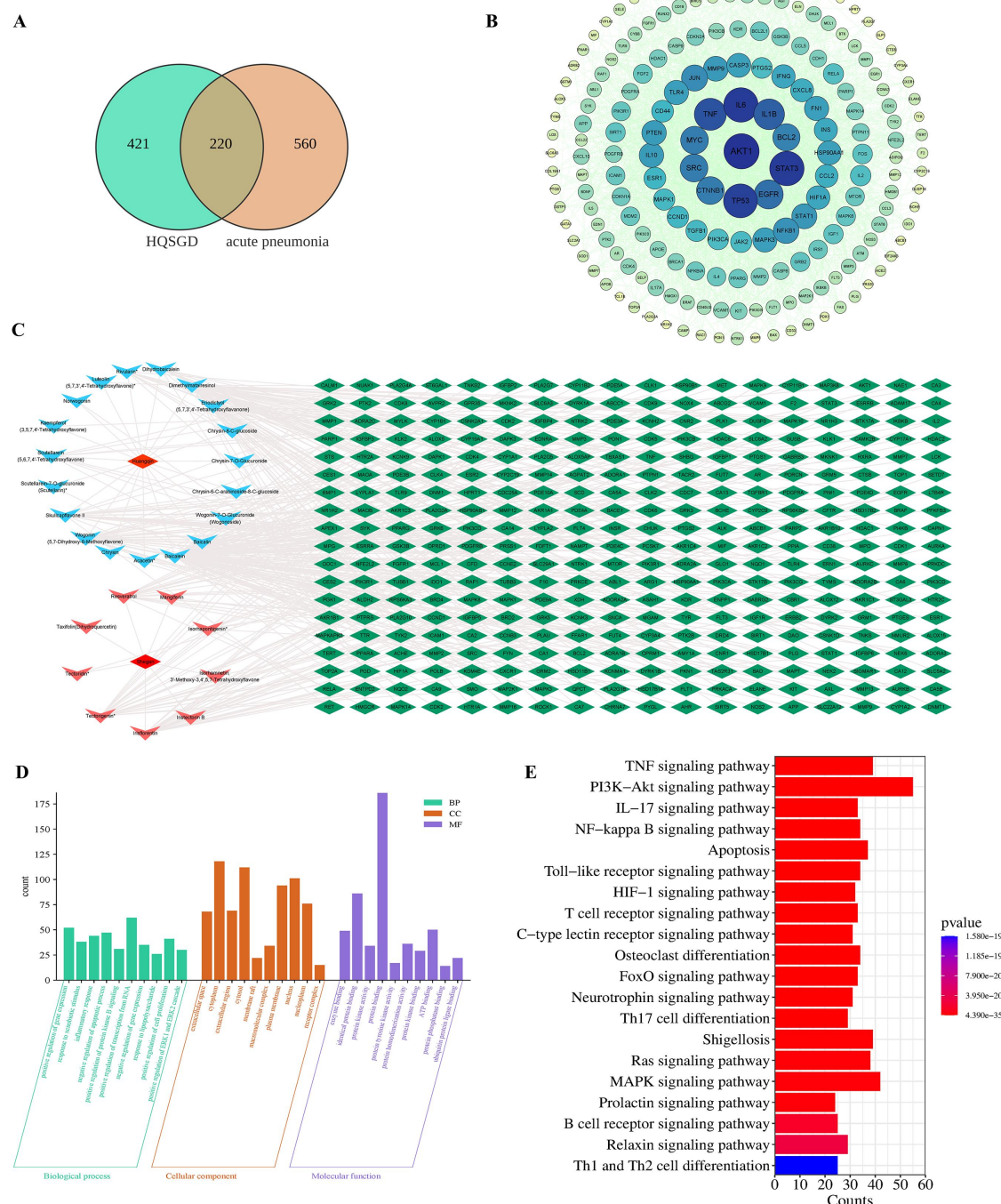


**Figure 5 Network pharmacology.** (A) Venn diagram demonstrating 220 overlapping target genes. (B) PPI network of overlapping genes. (C) Active compound-target network. (D) GO functional annotation analysis of potential therapeutic targets. (E) KEGG pathway enrichment analysis of potential therapeutic targets. HQSGD, Huangqin Shegan Decoction.



### RNA-Seq analysis

For RNA-seq, lung tissue specimens were procured from rats in the control, model, and high-dose HQSGD cohorts. As shown in the principal component analysis plot in Figure 6A, the gene expression profiles of the three cohorts differed notably, ensuring the accuracy of subsequent differential expression analysis. Based on  $|\log_2FC|$  values of  $> 1$  and FDR values of  $< 0.05$ , a sum of 2,947 DEGs, encompassing 1,090 increased, and 1,884 decreased genes, were determined between the control and model cohorts. Similarly, a sum of 2,588 DEGs, encompassing 1,662 increased and 926 decreased genes, were determined between the model and high-dose HQSGD cohorts (Figure 6B). These DEGs were visualized on heat maps and volcano plots

(Figure 6C–6F). GO and KEGG pathway enrichment analyses were conducted to compare the control vs. model cohort and the model vs. high cohort in Figure 7A–7D. The top 20 KEGG pathways linked to the DEGs were visualized and intersected with the top 20 KEGG pathways linked to the target genes utilizing a Venn diagram. Five overlapping pathways were identified, namely, TNF, NF- $\kappa$ B, PI3K-AKT, HIF-1, and MAPK signaling pathways (Figure 7E). KEGG analysis showed that the PI3K-AKT and NF-kappa B pathways were essential in the mechanism of action of HQSGD in AP. Mapping the PI3K-AKT pathway revealed its upstream and downstream interactions within the PI3K/AKT/NF- $\kappa$ B signaling cascade. Therefore, proteins and mRNAs linked to the PI3K-AKT and NF-kappa B pathways were further validated.

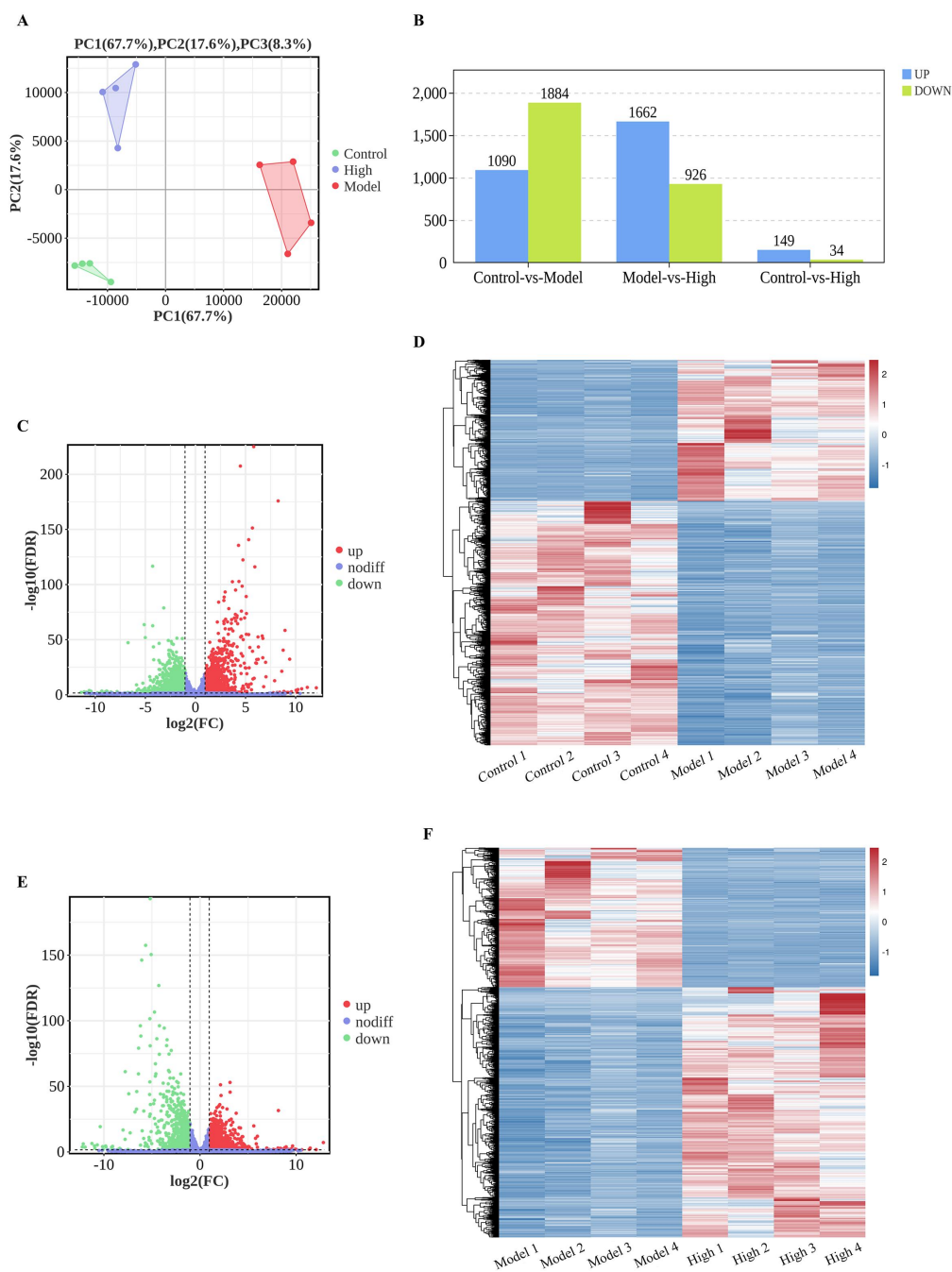


**Figure 6** Transcriptomic analysis of rat lung tissues. (A) Principal component analysis plot. (B) Identification of differentially expressed genes between groups. (C) Volcano plot demonstrating differentially expressed genes between the control and model groups. (D) Heat map demonstrating differentially expressed genes between the control and model groups. (E) Volcano plot demonstrating differentially expressed genes between the model and high-HQSGD groups. (F) Heat map demonstrating differentially expressed genes between the model and high-HQSGD groups.

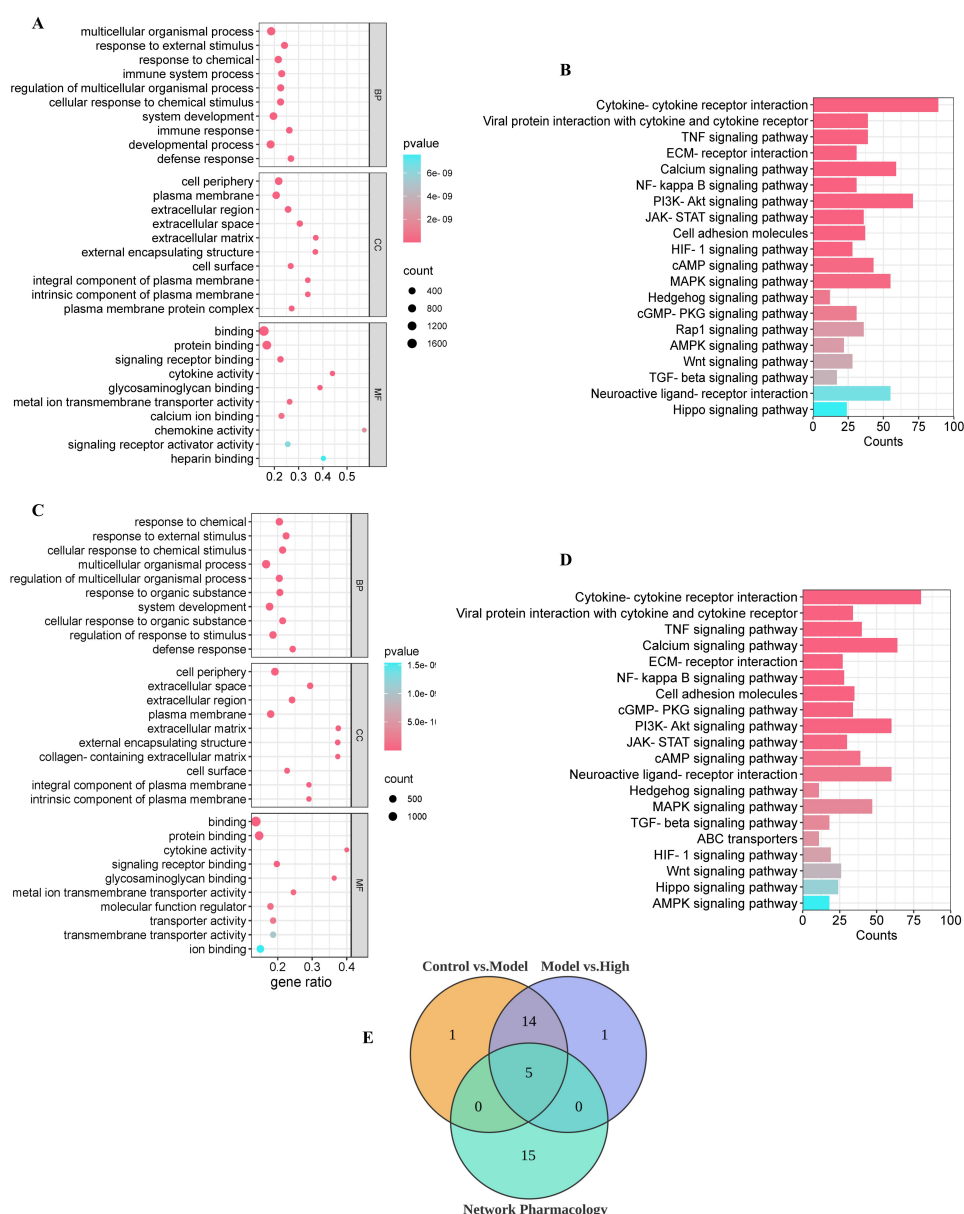


**Figure 7** GO and KEGG enrichment analyses after comparing groups. (A) GO enrichment analysis of differentially expressed genes between the control and model groups. (B) KEGG enrichment analysis of differentially expressed genes between the control and model groups. (C) GO enrichment analysis of differentially expressed genes between the model and high-HQSGD groups. (D) KEGG enrichment analysis of differentially expressed genes between the model and high-HQSGD groups. (E) Three sets of Venn diagrams that take the intersections into account.

#### Effect of HQSGD on the expression of PI3K/AKT/NF- $\kappa$ B pathway-related proteins in lung tissue of rats with AP

Based on the results of NP and transcriptomic sequencing, the good separation of the groups is clearly shown in Figure 8A. It shows that these three groups are significantly different on the main variables. The PI3K/AKT/NF- $\kappa$ B pathway was implicated in the action mechanism of HQSGD in the treatment of AP. As shown in Figure 8B–8D, the proportions of p-PI3K/PI3K, p-AKT/AKT, and p-NF- $\kappa$ B/NF- $\kappa$ B proteins in lung tissues were notably elevated in the model cohort relative to the control cohort ( $P < 0.01$ ). Nevertheless, these proportions were markedly reduced in the AZM cohort and the three HQSGD cohorts than in the model cohort ( $P < 0.05$ ,  $P < 0.01$ ).

#### Effect of HQSGD on mRNA expression of key genes in rats with AP

The mRNA expression of the three crucial genes, *PI3K*, *AKT*, and *NF- $\kappa$ B*, was verified through q-PCR, using *GAPDH* as the internal reference. The results showed that the mRNA expression of *PI3K*, *AKT*,

and *NF- $\kappa$ B* was notably elevated in the model cohort relative to the control cohort but significantly lower in the AZM cohort and the three HQSGD cohorts than in the model cohort (Figure 9).

#### Discussion

TCM attributes pneumonia primarily to the invasion of warmth and heat into the lungs. The core pathological conditions of pneumonia involve wind-heat and phlegm-heat. Therefore, treatment typically focuses on clearing lung heat, relieving external symptoms, and eliminating heat, phlegm, and toxins from the body [32]. Excessive inflammatory responses in the lungs disrupt the normal function of the airway, cilia, and alveolar epithelium [1]. HQSGD, listed in volume XII of the *Classical Compilation of Medical Notes* (Formulae for Pharyngeal and Throat Disorders), is known for its affinity for the lung meridian. It is frequently used to clear lung heat and is considered a key treatment agent for cough caused by lung heat. Shegan is commonly prescribed for conditions such as fever, phlegm-heat

patterns, sore throat, cough, and asthma. It possesses heat-clearing and detoxifying properties and can dispel phlegm and promote sweating. The combination of Huangqin and Shegan effectively clears heat and toxins from the lungs and stomach, alleviates congestion, and relieves throat symptoms, thereby exerting synergistic therapeutic effects against pneumonia [17, 33].

LPS, an endotoxin produced by Gram-negative bacteria, serves a crucial function in the inflammatory reaction to pneumonia in pediatric patients [34]. It has been shown to induce high expression of chemokines and inflammatory factors in various cell types in vivo and ex vivo. Therefore, LPS is commonly used to establish cell models of inflammation in studies on numerous diseases, including pneumonia [35, 36]. HQSGD has demonstrated promising therapeutic efficacy in pneumonia [37].

In this investigation, we developed a rat model of LPS-induced AP to evaluate the curative potential of HQSGD. Histopathological analysis showed that HQSGD reduced inflammatory cell infiltration in lung tissues and alleviated lung injury in rats with AP. Furthermore, HQSGD significantly increased the BW and decreased the lung index of rats with AP. Compared with the model cohort, the HQSGD-treated

cohorts had significantly lower levels of the inflammatory factors TNF- $\alpha$ , IL-1 $\beta$ , and CRP in the serum and significantly higher activity of SOD, an indicator of reduced oxidative stress, and lower expression of MDA in lung tissues.

NP and transcriptomic sequencing are common methods for investigating the mechanisms of action of drugs [38]. However, each method has inherent limitations and may yield false-positive results. Certain factors need to be considered when using these methods, such as the varying composition of herbs at different doses, alterations in the chemical composition of drugs after decoction, and discrepancies in the expression of disease-related genes between databases and animal models [39]. Therefore, we analyzed the chemical composition of HQSGD via UPLC-MS/MS and identified potent active compounds and their targets via NP. This approach was further integrated with transcriptomic analysis to enhance the reliability of the results. The results suggested that HQSGD exerted therapeutic effects against AP through modulation of the PI3K/AKT/NF- $\kappa$ B pathway. The PI3K pathway regulates redox reactions, inflammatory responses, apoptosis, and cell survival [40]. LPS-induced AP promotes activation of the PI3K pathway, which activates the NF- $\kappa$ B and MAPK pathways.

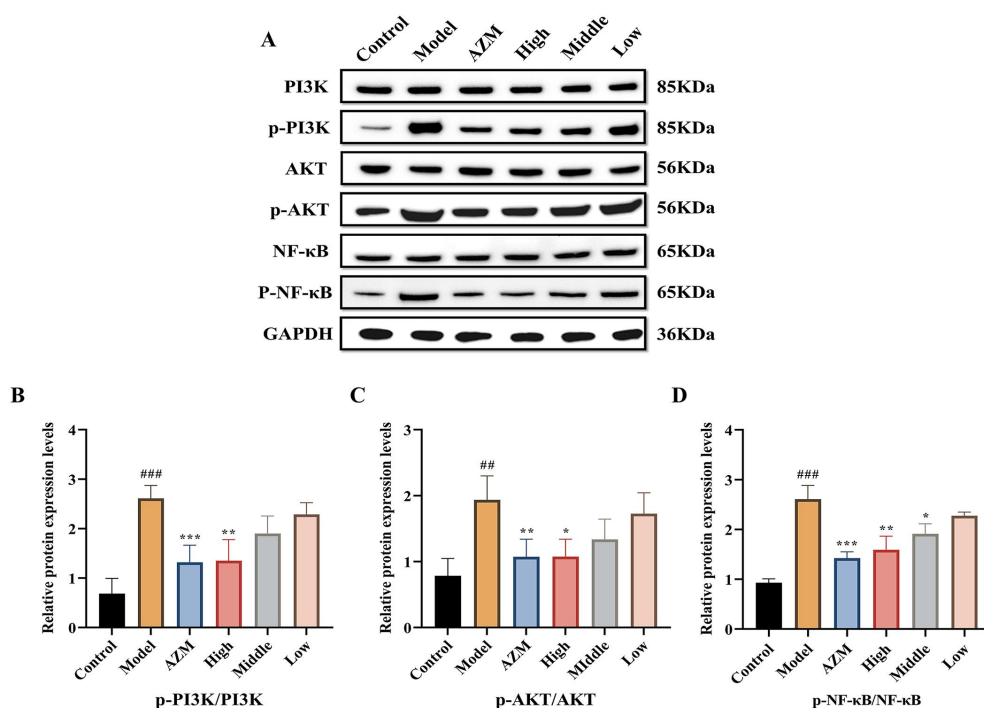


**Figure 8** HQSGD inhibited the PI3K/Akt/NF- $\kappa$ B pathway in acute pneumonia. (A) Protein expression of PI3K, AKT, and NF- $\kappa$ B in rat lung tissues. (B–D) Statistical analysis of phosphorylated and total protein levels of PI3K, AKT, and NF- $\kappa$ B. ## $P$  < 0.01, ### $P$  < 0.001 vs control group; \* $P$  < 0.05, \*\* $P$  < 0.01, \*\*\* $P$  < 0.001 vs model group;  $n$  = 3.

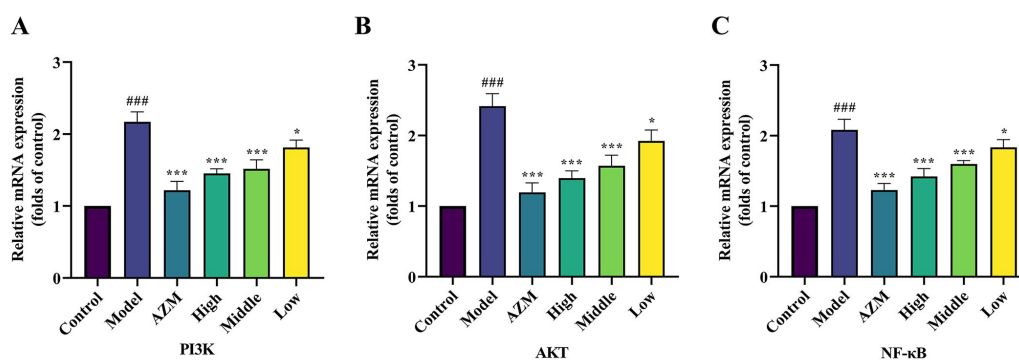


**Figure 9** The mRNA expression of PI3K, A-KT, and NF- $\kappa$ B in different groups was determined via q-PCR. ### $P$  < 0.001 vs control group; \* $P$  < 0.05, \*\*\* $P$  < 0.001 vs model group;  $n$  = 3.

These pathways have modulated the transcription of antioxidant and inflammatory factors. As a crucial cell signaling pathway, AKT regulates cell proliferation, metabolism, and inflammatory responses. AP-induced lung injury upregulates the AKT signaling pathway, and subsequent activation of related pathways, such as NF- $\kappa$ B, enhances the inflammatory response, further exacerbating the condition [41]. NF- $\kappa$ B is positioned in the signaling cascade subsequent to AKT. Upon activation, an inhibitor of kappa B kinase (IKK) phosphorylates and degrades I $\kappa$ B. NF- $\kappa$ B dissociates from I $\kappa$ B and translocates to the nucleus, where it interacts with additional transcriptional regulators to modulate the expression of genes associated with inflammation, immunity, and various other processes [42, 43]. The PI3K/AKT/NF- $\kappa$ B pathway is crucial in the development of bacterial pneumonia. Pathogenic bacteria can upregulate apoptotic proteases, leading to immune cell apoptosis. This event triggers a conformational change in PI3K and activates it, promoting the binding and phosphorylation of AKT and other PI3K activation messengers. Consequently, the downstream NF- $\kappa$ B pathway is stimulated, triggering an overproduction of pro-inflammatory mediators encompassing IL-1 $\beta$ , IL-6, and TNF- $\alpha$ , which exacerbate local tissue damage [44–47]. In this study, western blotting showed that HQSGD decreased the protein expression of PI3K, AKT, and NF- $\kappa$ B in the lung tissues of rats with AP. HQSGD's suppression of the PI3K/AKT/NF- $\kappa$ B signaling cascade mitigated the secretion of subsequent inflammatory factors, thereby alleviating inflammatory damage in lung tissues.

In recent years, numerous in vitro and in vivo experimental investigations have validated that the PI3K/AKT signaling pathway exerts an inhibitory influence on lung inflammatory responses [48–50]. In addition, research has demonstrated that the PI3K/AKT/NF- $\kappa$ B cascade is crucial in oxidative stress and inflammatory responses in AP models [51, 52]. Regulating the expression of the PI3K/AKT pathway facilitates the transcription of various downstream antioxidant factors. On the contrary, suppressing the NF- $\kappa$ B pathway suppresses the synthesis and release of pro-inflammatory mediators like TNF- $\alpha$ , HIF- $\alpha$ , and IL-1 $\beta$ . Therefore, drugs targeting the PI3K/AKT/NF- $\kappa$ B signaling pathway hold substantial potential in the treatment of AP [49, 51, 52]. However, studies investigating the PI3K/AKT/NF- $\kappa$ B pathway at the molecular level are limited at present, and the relationship among downstream factors involved in this pathway warrants further investigation [50, 53, 54]. The treatment of AP requires rapid and effective intervention, and the onset of action of TCM may be slower, which may not be suitable as the first choice of treatment for AP. Therefore, the application of HQSGD in the treatment of AP may be limited by its traditional indications, the diversity of pathogens, the severity of the disease, and the availability and effectiveness of modern medical treatments.

In the treatment of AP, TCM can serve as a complementary approach to modern medical therapy. The integration of TCM with Western medical treatments may demonstrate enhanced efficacy.

## Conclusions

In summary, this research showed that treatment with high-dose HQSGD substantially alleviated lung damage in rats with AP. Mechanistically, HQSGD potentially exhibits anti-inflammatory characteristics through its suppression of the PI3K/AKT/NF- $\kappa$ B pathway. Nonetheless, the precise processes by which HQSGD modulates the PI3K/AKT/NF- $\kappa$ B signaling cascade and its downstream molecules in the treatment of AP remain unclear. Elucidating these mechanisms may provide novel avenues for expanding the clinical application of HQSGD.

## References

- Corrales-Medina VF, Musher DM, Shachkina S, Chirinos JA. Acute pneumonia and the cardiovascular system. *Lancet*. 2013;381(9865):496–505. Available at: [https://doi.org/10.1016/s0140-6736\(12\)61266-5](https://doi.org/10.1016/s0140-6736(12)61266-5)

- Qin YL. Acute pneumonia in correspondence teaching materials of traditional Chinese medicine in the Republic of China. *J Tradit Chin Med Lit*. 2020;38(6):19–21. (Chinese) Available at: [https://kns.cnki.net/kcms2/article/abstract?v=amOBmv6QLToiqPwnNDw7YZYZ1g57Mm-ua3M9gZnGF13A\\_40\\_f1NB-E17Dvm3LN4Dla7GFborN3-XGqbyVCa6HFE7VgCuLaVyB1ABYVobfLDvUUHa33VSDCih75tr5okRM6NYWvA7Fi83ngc83VZ\\_h9PIn93RL-LMwKpyBqlhpKpwp7scfjJkC7NFxF6Fa1JcAS\\_T\\_FCAA=&unipl](https://kns.cnki.net/kcms2/article/abstract?v=amOBmv6QLToiqPwnNDw7YZYZ1g57Mm-ua3M9gZnGF13A_40_f1NB-E17Dvm3LN4Dla7GFborN3-XGqbyVCa6HFE7VgCuLaVyB1ABYVobfLDvUUHa33VSDCih75tr5okRM6NYWvA7Fi83ngc83VZ_h9PIn93RL-LMwKpyBqlhpKpwp7scfjJkC7NFxF6Fa1JcAS_T_FCAA=&unipl)
- Tang J, Lu Y, Long ZH, et al. Study on the protective effect of sinew grass decoction on acute pneumonia. *J North Sichuan Med College*. 2017;32(3):329–331. (Chinese) Available at: <http://doi.org/10.3969/j.issn.1005-3697.2017.03.004>
- Jin WB. Protective effect of resveratrol on lipopolysaccharide-induced severe pneumonia in mice. *Chin J Clin Pharmacol Ther*. 2011;16(12):1352–1356. (Chinese) Available at: <https://kns.cnki.net/kcms2/article/abstract?v=amOBmv6QLTpxhEK9wrmruLApx4jpfgrBp2X0rAwT5GwMp4JFQsqHanIWS3eX-nA1QOJrsSFGDvxquzq7Ekz8RarMSDgbQ114bHiaCOXmbLhzkFZ6Mh8qNuBTrgFke4WSNSshyIUBtnhv82AXGwM90yIGIwS0M91FJgNDilMPnM1m6ff80DSa2yg4Zhxma&uniplatform=NZKPT>
- Chen JG, Cui W. Weng Zao and “Medical Compendium”. *J Changchun Univ Tradit Chin Med*. 2013;29(4):748–749. (Chinese) Available at: <http://doi.org/10.13463/j.cnki.cczyy.2013.04.004>
- Zheng YF, Wang JJ, Fu C, Wang JX. Progress of research on the chemical composition and pharmacological effects of *Scutellaria baicalensis*. *Chin Tradit Pat Med*. 2016;38(1):141–147. (Chinese) Available at: <https://kns.cnki.net/kcms2/article/abstract?v=9g5ITc5ddu1Xjo9Low7Z9Pk2smp-AyzBITek2EpGtG0NN24YTI-vZdNfwXZenO24w7W1q-2cghmS4-oeofQIUOkuywbaRBUszwdMq20VCGvrMaQubOvne7cpMFGxFTQTilxalymMgHEdlnFBebIliw65IJSJkKfXfo2zAOmfUT-7nxhX6A07y17iWujdFT&uniplatform=NZKPT>
- Wu ZS, Ji P, Wei YM, et al. Protective effect of *Scutellaria Huangqin-Lianqiao* combination on lipopolysaccharide-induced acute pneumonia model in mice. *Acta Lab Anim Sci Sin*. 2022;30(6):800–809. (Chinese) Available at: <http://doi.org/10.3969/j.issn.1005-4847.2022.06.009>
- Wang LB. Fundamental study on the in vivo effect substances of catechu-scutellariae allotment. Northwest Agriculture and Forestry University. 2019. (Chinese) Available at: [https://kns.cnki.net/kcms2/article/abstract?v=th5-mUcNEOMgEl00Qa8a5zGM3DJ62x3fP9KRSIkZr60jNA89rww0T8DpMzIqnllSwVc\\_xBNZsL65F0gY5vIbgnS6isGUJ0pX7ziPIH2UzZiCEExYyh0LT5C6eKJJiif3kCKtMBZb0mRZO\\_IKVOFKebCqUPkrMUAP8ijzkDdnT8uY5Lfmryfak2MI7EvLnBvXubAIZOX7A=&unipl](https://kns.cnki.net/kcms2/article/abstract?v=th5-mUcNEOMgEl00Qa8a5zGM3DJ62x3fP9KRSIkZr60jNA89rww0T8DpMzIqnllSwVc_xBNZsL65F0gY5vIbgnS6isGUJ0pX7ziPIH2UzZiCEExYyh0LT5C6eKJJiif3kCKtMBZb0mRZO_IKVOFKebCqUPkrMUAP8ijzkDdnT8uY5Lfmryfak2MI7EvLnBvXubAIZOX7A=&unipl)
- Zhang L, Zhang N. Progress of chemical and pharmacological studies on *Szechuan shagan*. *J Shaanxi Univ Chin Med*. 2014;37(5):91–93. (Chinese) Available at: <http://doi.org/10.13424/j.cnki.jsctcm.2014.05.072>
- Shi YJ, Zhang Y, Gan Y, et al. Effect of Sjogren's cough capsule on the intestinal flora of methicillin-resistant *Staphylococcus aureus*-infected rats with pneumonia based on the theory of “the lung and the large intestine are mutually exclusive”. *Chin Arch Tradit Chin Med*. 2024;42(11):55–60 + 271–276. (Chinese) Available at: <http://doi.org/10.13193/j.issn.1673-7717.2024.11.012>
- Chen Y. Analysis of the efficacy of shooting hemp oral solution combined with budesonide suspension for inhalation in the treatment of asthmatic pneumonia. *J Med Theory Pract*. 2023;36(13):2208–2211. (Chinese) Available at: <http://doi.org/10.19381/j.issn.1001-7585.2023.13.015>
- Zhang RZ, Zhu X, Bai H, Ning K. Network pharmacology databases for traditional Chinese medicine: Review and assessment. *Front Pharmacol*. 2019;10:123. Available at: <http://doi.org/10.3389/fphar.2019.00123>



13. Finotello F, Di Camillo B. Measuring differential gene expression using RNA-seq: challenges and strategies for data analysis. *Brief Funct Genomics*. 2015;14(2):130–142. Available at: <http://doi.org/10.1093/bfpg/elu035>
14. Zhu HH, Wang S, Shan C, et al. Mechanism of the protective effect of xuan-bai-cheng-qi decoction on LPS-induced acute lung injury based on an integrated network pharmacology and RNA sequencing approach. *Respir Res*. 2021;22(1):188. Available at: <http://doi.org/10.1186/s12931-021-01781-1>
15. Cheng RX, Wu HQ, Ye XH, et al. Exploring the mechanism of cardiac yin tablets against chronic heart failure based on transcriptomics and network pharmacology. *Tradit Chin Drug Res Clin Pharmacol*. 2022;33(8):1083–1092. (Chinese) Available at: <http://doi.org/10.19378/j.issn.1003-9783.2022.08.011>
16. Wang XS. Study on the mechanism of action of ginseng against diabetic kidney injury based on metabolomics and transcriptomics. Jilin University. 2023. (Chinese) Available at: <http://doi.org/10.27162/d.cnki.gjlin.2023.000875>
17. Yin JT, Wang XY, Gu X, Zhang Y, Li GX. Molecular docking study of isoflavonoid components and MAPK signalling pathway in Huangqin Shegan Decoction. *Chin Arch Tradit Chin Med*. 2020;38(10):52–54 + 269–270. (Chinese) Available at: <http://doi.org/10.13193/j.issn.1673-7717.2020.10.012>
18. Liu Z. Molecular docking of main flavonoid components of Huangqin Shegan Decoction with neuraminidase of H7N9 virus. *Chin Arch Tradit Chin Med*. 2020;17(3):110–116. (Chinese) Available at: [https://kns.cnki.net/kcms2/article/abstract?v=th5-mUcNE00Na80TE9MS6TESIFRblunleA8XYsQUL4mOXF81WOTbrXHdsm-s-fpAFXxewK9y9Si-qDyQ-w8PIMa9yu4m6S\\_VrJ70KQNxjUokTuSHYUbyVqWC2ToaIoIn5fPE2hnITA4nDSOgfJZV0izt\\_hO5mkgh\\_b73849Yx-UzCYPsBMoo6AGxkAGImej6qx-RE-UL8=&unipl](https://kns.cnki.net/kcms2/article/abstract?v=th5-mUcNE00Na80TE9MS6TESIFRblunleA8XYsQUL4mOXF81WOTbrXHdsm-s-fpAFXxewK9y9Si-qDyQ-w8PIMa9yu4m6S_VrJ70KQNxjUokTuSHYUbyVqWC2ToaIoIn5fPE2hnITA4nDSOgfJZV0izt_hO5mkgh_b73849Yx-UzCYPsBMoo6AGxkAGImej6qx-RE-UL8=&unipl)
19. Lu J, Ren M, Gao LM, Zhang Y, Zhao Y. Study on the antibacterial effect of Huangqin Shegan Decoction on MRSA and the preliminary mechanism of action. *J Pract Chin Med Int Med*. 2023;37(11):68–70 + 159. (Chinese) Available at: <http://doi.org/10.13729/j.issn.1671-7813.Z20221726>
20. Yang XY. Efficacy and safety of azithromycin sequential therapy in the treatment of paediatric mycoplasma pneumonia. *J Clin Ration Use Drugs*. 2020;13(10):86–87. (Chinese) Available at: <http://doi.org/10.15887/j.cnki.13-1389/r.2020.10.050>
21. Qin L, Luan ZX, Li M, Xiang Y, Qi XR. Astragalus-danshen modulates autophagy through PI3K/Akt/mTOR pathway to ameliorate acute lung injury in rats. *China J Chin Mater Med*. 2024;49(12):3295–3301. (Chinese) Available at: <http://doi.org/10.19540/j.cnki.cjcm.20240207.402>
22. Zhang ML, Wu FF, Tan ZN, et al. Anti-inflammatory effect of anise compound on lipopolysaccharide-induced acute pneumonia model rats. *Chin J Emerg Tradit Chin Med*. 2023;32(6):951–953 + 991. (Chinese) Available at: <http://doi.org/10.3969/j.issn.1004-745X.2023.06.003>
23. Zhang Y, Wang XY, Wen W, Li GX. Expression of ROR $\gamma$ t in lung tissues of rats with post-infectious cough and the interventional effect of Huangqin Shegan Decoction it. *Chin J New Drugs*. 2019;28(4):418–422. (Chinese) Available at: [https://kns.cnki.net/kcms2/article/abstract?v=th5-mUcNE0PQM-FP6yp8-AG8qnXcHoQmTo-eUA1vwN7wNprdT5JZwrjqLYRy3YUxnft5IXtuKAqTduaCLzxr4jX\\_e\\_bFUnM8GBIqdyDO-Q8bdyqnTSWanu1ZSQmoJx-DrxIQffqN1AdWz6xv2iKE88XL6NQ4N0PIfTE2GP1LYvuJW9E-hEbZKdMJ44rvMCzjB1kFH6YyE=&unipl](https://kns.cnki.net/kcms2/article/abstract?v=th5-mUcNE0PQM-FP6yp8-AG8qnXcHoQmTo-eUA1vwN7wNprdT5JZwrjqLYRy3YUxnft5IXtuKAqTduaCLzxr4jX_e_bFUnM8GBIqdyDO-Q8bdyqnTSWanu1ZSQmoJx-DrxIQffqN1AdWz6xv2iKE88XL6NQ4N0PIfTE2GP1LYvuJW9E-hEbZKdMJ44rvMCzjB1kFH6YyE=&unipl)
24. Lu J, Ren M, Gao LM, Zhang Y, Zhao Y. Study on the antibacterial effect and preliminary mechanism of action of Huangqin Shegan Decoction on MRSA. *J Pract Chin Med*. 2023;37(11):68–70 + 159. (Chinese) Available at: <http://doi.org/10.13729/j.issn.1671-7813.Z20221726>
25. Chen W, Gong L, Guo Z, et al. A Novel Integrated Method for Large-Scale Detection, Identification and Quantification of Widely Targeted Metabolites: Application in the Study of Rice Metabolomics. *Mol Plant*. 2013;6(6):1769–1780. Available at: <http://doi.org/10.1093/mp/sst080>
26. Fraga CG, Clowers BH, Moore RJ, et al. Signature-discovery approach for sample matching of a nerve-agent precursor using liquid chromatography-mass spectrometry, XCMS, and chemometrics. *Anal Chem*. 2010;82(10):4165–4173. Available at: <http://doi.org/10.1021/ac1003568>
27. Wang B, Wang XL, Li LX, et al. Exploring the mechanism of action of ginseng and yi heart granules in the treatment of heart failure based on network pharmacology, molecular docking and experimental validation. *Tradit Chin Drug Res Clin Pharmacol*. 2024;35(9):1352–1363. (Chinese) Available at: <http://doi.org/10.19378/j.issn.1003-9783.2024.09.009>
28. He JF, Zhang D, Zheng JK, Zhang Y, Jin YH, Yan J. Exploration of the mechanism of action of astragalus-leech drug pairing for the treatment of pulmonary fibrosis based on network pharmacology. *Modern Chin Med*. 2022;24(1):59–69. (Chinese) Available at: <http://doi.org/10.13313/j.issn.1673-4890.20201223007>
29. He ZL, Ren RN, Wang F, et al. Mechanism of action of Sangju Drink in the treatment of acute lung injury based on UHPLC-ESI-QTOF-MS/MS compositional analysis, network pharmacology and experimental validation. *Drug Eval Res*. 2024;47(10):2227–2240. (Chinese) Available at: [https://kns.cnki.net/kcms2/article/abstract?v=9g5lTc5ddu0kQe5leh1w6\\_pXrliDfck3p5yFQKEyIhRympzrrdxwZAIvDtJrtKQBaoaIJh0eHGgX3OMBKc\\_VWJEK8188B8kgx5XWVM4sgQCu4Vh\\_c3i2tIje\\_kCCJVV8NjigUsk\\_JyCnPz9\\_zcjCifHAGtO8yJq6TMh-GTfiWxf2FVUKNWS7yAlk4rmZpmXTtheDh8Sk=&unipl](https://kns.cnki.net/kcms2/article/abstract?v=9g5lTc5ddu0kQe5leh1w6_pXrliDfck3p5yFQKEyIhRympzrrdxwZAIvDtJrtKQBaoaIJh0eHGgX3OMBKc_VWJEK8188B8kgx5XWVM4sgQCu4Vh_c3i2tIje_kCCJVV8NjigUsk_JyCnPz9_zcjCifHAGtO8yJq6TMh-GTfiWxf2FVUKNWS7yAlk4rmZpmXTtheDh8Sk=&unipl)
30. Jiang YJ, Cui YH, Li DL, Yu XF. Revealing the mechanism of Xiao Chaihu Tang in treating Mycoplasma pneumonia and its relationship with pulmonary epidemics based on network pharmacology and molecular docking. *Hunan J Tradit Chin Med*. 2024;40(9):181–189. (Chinese) Available at: <http://doi.org/10.16808/j.cnki.issn1003-7705.2024.09.039>
31. Huang YL, Wang Y, Wang GH, Zhou TT, Zhang WJ. Exploring the mechanism of action of groundnut branches and leaves in the treatment of insomnia based on network pharmacology and animal experiments. *Chin Tradit Herb Drugs*. 2024;55(21):7347–7358. (Chinese) Available at: [https://kns.cnki.net/kcms2/article/abstract?v=9g5lTc5ddu1g9D5g7VSAQ7b7UGxjJlt8R\\_MJ5IyUcDyS3LODhHB983OZVfvNvETHh4Nk2SN\\_LBLuD0KbkA7F-hAotHLjtaV1OgG8AFP-cHpa4q35WPmmpC2tkZpDLZDo1WsRYaCTcEg-u3-1yF7mCz4CsAtcrpgCOowFXhydSz2gbPGX1a5klvkeAD2Dpone&uniplatform=NZKPT](https://kns.cnki.net/kcms2/article/abstract?v=9g5lTc5ddu1g9D5g7VSAQ7b7UGxjJlt8R_MJ5IyUcDyS3LODhHB983OZVfvNvETHh4Nk2SN_LBLuD0KbkA7F-hAotHLjtaV1OgG8AFP-cHpa4q35WPmmpC2tkZpDLZDo1WsRYaCTcEg-u3-1yF7mCz4CsAtcrpgCOowFXhydSz2gbPGX1a5klvkeAD2Dpone&uniplatform=NZKPT)
32. Hu XG. Traditional Chinese medicine treatment of Mycoplasma pneumoniae. *Fam Med*. 2023;12:52–53. (Chinese) Available at: [https://kns.cnki.net/kcms2/article/abstract?v=th5-mUcNE0P1vzHVBCBw63\\_9r0xSonmeUPoWFan-xHhFqvmvYEAvbTgskIY3qhIS5\\_pHC\\_vDmlBwyhhetuivxAtwz4BRE1amiwMo6LHr-ezsv3O\\_pz9iFAEiROhPKY4tdUXnQnGSOYtCkBRq1gWWz70WimybcTgl-7LgHsY\\_ELK62MexQIOO97cJ-c-hczm898TSITyPQ=&unipl](https://kns.cnki.net/kcms2/article/abstract?v=th5-mUcNE0P1vzHVBCBw63_9r0xSonmeUPoWFan-xHhFqvmvYEAvbTgskIY3qhIS5_pHC_vDmlBwyhhetuivxAtwz4BRE1amiwMo6LHr-ezsv3O_pz9iFAEiROhPKY4tdUXnQnGSOYtCkBRq1gWWz70WimybcTgl-7LgHsY_ELK62MexQIOO97cJ-c-hczm898TSITyPQ=&unipl)
33. Li QL, Peng J, Zhou BH, Xu H. Exploring the mechanism of anti-inflammatory effect of Huangqin Shegan Decoction in the treatment of paediatric pneumonia based on network pharmacology and experimental validation. *Cent South Pharm*. 2023;21(8):2009–2015. (Chinese) Available at: [https://kns.cnki.net/kcms2/article/abstract?v=UbUZFcLhZJL-m9icqOUFH1Fe81NVNJV\\_c7vQGR64NJ\\_7i7Pq2QeAtXp3JNgigtudv8RUhKV9xMI-rq1yoyWfLwTdTS58O775mWdsCtaMwmpz637VgDEIDcOTwOTVJ6pQauFUepmOSDBKi26Y4xgWp8LzqXGPl461hfx\\_19z5D6u56C5ebzFsdM3SWopAgkwIleozLU\\_Mmjw=&unipl](https://kns.cnki.net/kcms2/article/abstract?v=UbUZFcLhZJL-m9icqOUFH1Fe81NVNJV_c7vQGR64NJ_7i7Pq2QeAtXp3JNgigtudv8RUhKV9xMI-rq1yoyWfLwTdTS58O775mWdsCtaMwmpz637VgDEIDcOTwOTVJ6pQauFUepmOSDBKi26Y4xgWp8LzqXGPl461hfx_19z5D6u56C5ebzFsdM3SWopAgkwIleozLU_Mmjw=&unipl)
34. Liu Q, Yang H, Xu SN, Sun XM. Downregulation of p300

- alleviates LPS-induced inflammatory injuries through regulation of Rho A/ROCK/NF-kappa B pathways in A549 cells. *Biomed Pharmacother.* 2018;97:369–374. Available at: <http://doi.org/10.1016/j.biopha.2017.10.104>
35. Zhou JT, Ren KD, Hou J, Chen J, Yang G. a-rhamnrtin-3-a-rhamnoside exerts anti-inflammatory effects on lipopolysaccharide-stimulated RAW264.7 cells by abrogating NF-kB and activating the Nrf2 signaling pathway. *Mol Med Rep.* 2021;24(5):799. Available at: <http://doi.org/10.3892/mmr.2021.12439>
  36. Wang P, Zhang HT, Zhao WQ, Dai NN. Silencing of long non-coding RNA KCNQ10T1 alleviates LPS-induced lung injury by regulating the mi R-370-3p/FOXO1 axis in childhood pneumonia. *BMC Pulm Med.* 2021;21(1):247. Available at: <http://doi.org/10.1186/s12890-021-01609-0>
  37. Wang XY. Research on anti-inflammatory mechanism and quality control of Huangqin Shegan Decoction based on molecular docking. Liaoning University of Traditional Chinese Medicine. 2020. (Chinese) Available at: <http://doi.org/10.27213/d.cnki.glnzc.2019.000510>
  38. Wang P. Exploration of the mechanism of endometriosis in the treatment of endometriosis based on network pharmacology and transcriptomics. Guangzhou University of Traditional Chinese Medicine. 2023. (Chinese) Available at: <http://doi.org/10.27044/d.cnki.ggzcu.2023.000005>
  39. Guo JN, Liang JM, Guo ZY, et al. Network pharmacology and transcriptomics to determine Danggui Yifei Decoction mechanism of action for the treatment of chronic lung injury. *J Ethnopharmacol.* 2024;318:116873. Available at: <http://doi.org/10.1016/j.jep.2023.116873>
  40. Huang P, Guo YH, Xu XL, He SS, Liu QQ. The role of PI3K/Akt/mTOR signalling pathway in regulating Treg/Th17 balance in severe pneumonia and the progress of research in traditional Chinese medicine. *J Emerg Tradit Chin.* (Chinese) 2018;27(12):2245–2247. Available at: <http://doi.org/10.3969/j.issn.1004-745X.2018.12.057>
  41. Li CY, Wang DZ, Zhang B, Su XY, Wang DS. Exploring the mechanism of metformin on lung injury in rats with stroke-associated pneumonia based on leptin-mediated PI3K/AKT pathway. *Chin J Integr Med Cardio Cerebrovasc Dis.* 2024;22(9):1604–1609. (Chinese) Available at: <http://doi.org/10.12102/j.issn.1672-1349.2024.09.011>
  42. Giridharan S, Srinivasan M. Mechanisms of NF-kB p65 and strategies for therapeutic manipulation. *J Inflamm Res.* 2018;11:407–419. Available at: <http://doi.org/10.2147/jir.s140188>
  43. Wang XF, Gao S, Hao ZX, Tang T, Liu FS. Involvement of TRAF6 in regulating immune defense and ovarian development in *Musca domestica*. *Int J Biol Macromol.* 2020;153:1262–1271. Available at: <http://doi.org/10.1016/j.ijbiomac.2019.10.259>
  44. Li D, Guo Y, Cen X, et al. Lupeol protects against cardiac hypertrophy via TLR4-PI3K-Akt-NF-kB pathways. *Acta Pharmacol Sin.* 2022;43(8):1989–2002. Available at: <http://doi.org/10.1038/s41401-021-00820-3>
  45. Rueda ZV, Aguilar Y, Maya MA, et al. Etiology and the challenge of diagnostic testing of community-acquired pneumonia in children and adolescents. *BMC Pediatr.* 2022;22(1):169. Available at: <http://doi.org/10.1186/s12887-022-03235-z>
  46. Jia XL, Gu MD, Dai JQ, et al. Quercetin attenuates *Pseudomonas aeruginosa*-induced acute lung inflammation by inhibiting PI3K/AKT/NF-kB signaling pathway. *Inflammopharmacology.* 2024;32(2):1059–1076. Available at: <http://doi.org/10.1007/s10787-023-01416-5>
  47. Kim SW, Jee W, Park SM, et al. Anti-inflammatory Effect of *Symplocos prunifolia* Extract in an In Vitro Model of Acute Pneumonia. *Plant Foods Human Nutr.* 2024;79(4):893–900. Available at: <http://doi.org/10.1007/s11130-024-01231-5>
  48. Jaeger JM, Titus BJ, Blank RS. Essential anatomy and physiology of the respiratory system and the pulmonary circulation. *Princ Pract Anesth Thorac Surg.* 2019;65–92. (Chinese) Available at: [http://doi.org/10.1007/978-3-030-00859-8\\_4](http://doi.org/10.1007/978-3-030-00859-8_4)
  49. Sun YL, Zhang DM, Hu F, Lu DM. Effects of respiratory pseudohyphae colonisation on severe bacterial ventilator-associated pneumonia and PI3K/Akt/NF-kB signalling pathway. *Chin J Nosocomiol.* 2023;33(7):1006–1010. (Chinese) Available at: [https://kns.cnki.net/kcms2/article/abstract?v=9g5lTc5ddu3YIsBCMLIPINI1Sdh-QCT\\_wjqCFVzUUIK9BOFFBJBcv2EynkMNuBJQByrNd9x5QktPvHBSNOrdChPfoCmsuP2b4HGm\\_x0nVouO-SrnewdpG4DrTWARfX4MnQFe00FRWKL1JQ-EUfxPYBodLL7Nce\\_BHwT1xn31rsX0bu9EupcOt-X\\_hYrXvf&uniplatform=NZKPT](https://kns.cnki.net/kcms2/article/abstract?v=9g5lTc5ddu3YIsBCMLIPINI1Sdh-QCT_wjqCFVzUUIK9BOFFBJBcv2EynkMNuBJQByrNd9x5QktPvHBSNOrdChPfoCmsuP2b4HGm_x0nVouO-SrnewdpG4DrTWARfX4MnQFe00FRWKL1JQ-EUfxPYBodLL7Nce_BHwT1xn31rsX0bu9EupcOt-X_hYrXvf&uniplatform=NZKPT)
  50. Liu S, Wang XF, Hao MW. The Influence of Qingfei Tongluo Ointment on PI3K/AKT/NF-kB p65 Protein Expression in Rat Lung Tissue with Type IV Pneumonia. *Chin Arch Tradit Chin Med.* 2017;35(9):2289–2291. (Chinese) Available at: <http://doi.org/10.13193/j.issn.1673-7717.2017.09.023>
  51. Li M, Wang L, Xia YF, Yan S. Exploring the protective effect of compound glycyrrhizin on lung injury in mice with viral pneumonia based on PI3K/Akt/NF-kB pathway. *Chin Tradit Pat Med.* 2023;45(11):3775–3779. (Chinese) Available at: <http://doi.org/10.3969/j.issn.1001-1528.2023.11.046>
  52. Wang L, Wang Y, Wu Q, Chen CM. Effect of miR-23b-3p regulating PI3K/Akt/NF-kB signalling pathway on imipenem-induced lung injury in rats with severe pneumonia. *Chin J Gerontol.* 2024;44(8):1930–1934. (Chinese) Available at: <http://doi.org/10.3969/j.issn.1005-9202.2024.08.036>
  53. Zhou B, Wang D, Sun G, et al. Effect of miR-21 on apoptosis in lung cancer cell through inhibiting the PI3K/Akt/NF-kB signaling pathway in vitro and in vivo. *Cell Physiol Biochem.* 2018;46(3):999–1008. Available at: <http://doi.org/10.1159/000488831>
  54. Hong L. Study on amelioration of LPS-induced acute lung injury by safranin based on inhibition of PI3K/Akt/NF-kB signalling pathway. China Medical University. 2018. (Chinese) Available at: [https://kns.cnki.net/kcms2/article/abstract?v=qINkJK8c4F\\_uuwD1VvK6Br1Oh3UHrnwph7rJD9lgql6khwvolDSO35WdsgSHp63-PuPuz7jd-xtF7au9nr6NruLQ4SLH7iyoEoWVGOH1h1Eb5lSK6tz9X0eJmqmtFLKRpABIErLEjZKv7ziD8y-ygbsnhQR6N\\_TijOp8SUX\\_XfhqvVpMLYBrT4vbUYaPxywP6VYfO8XQ=&unipl](https://kns.cnki.net/kcms2/article/abstract?v=qINkJK8c4F_uuwD1VvK6Br1Oh3UHrnwph7rJD9lgql6khwvolDSO35WdsgSHp63-PuPuz7jd-xtF7au9nr6NruLQ4SLH7iyoEoWVGOH1h1Eb5lSK6tz9X0eJmqmtFLKRpABIErLEjZKv7ziD8y-ygbsnhQR6N_TijOp8SUX_XfhqvVpMLYBrT4vbUYaPxywP6VYfO8XQ=&unipl)